A comparative study on aggregation/sedimentation of TiO_2 nanoparticles in mono- and binary systems of fulvic acids and Fe(III)

Si Li[a], Weiling Sun[b],*

[a] Key Laboratory for Urban Habitat Environmental Science and Technology, School of Environment and Energy, Peking University Shenzhen Graduate School, Shenzhen 518055, China
[b] Department of Environmental Engineering, Peking University, The Key Laboratory of Water and Sediment Sciences, Ministry of Education, Beijing 100871, China

ABSTRACT

The aggregation/sedimentation potentials of TiO_2 nanoparticles were studied in mono- and binary systems of Suwannee River fulvic acids (SRFA) and Fe(III) at different pH values. SRFA adsorption significantly enhanced the stability of TiO_2 nanoparticles at pH 4, 6 and 8, mainly due to the dramatic increase in negative surface charges. The presence of Fe(III) stabilized aggregation/sedimentation of TiO_2 nanoparticles at pH 4 due to the increasing positive charges after Fe(III) sorption, but destabilized aggregation/sedimentation at pH 6 and 8 attributed to the bridging effect of Fe(III)-hydroxy. The formation of COO–Fe(III) complex was found in binary system of SRFA and Fe(III). Thus, the positive charges that Fe(III) imparted to nanoparticles were neutralized by SRFA. Compared with those in mono-system of Fe(III), SRFA enhanced aggregation/sedimentation at pH 4, while stabilized TiO_2 nanoparticles at higher pH in binary system of SRFA and Fe(III). The sedimentation rates of TiO_2 nanoparticles showed relatively lower coefficient with zeta potentials (-0.883, $P < 0.01$) than with hydrodynamic particle sizes (0.964, $P < 0.01$), due to the steric hindrance of SRFA and the bridging effect of Fe(III)-hydroxy, which was confirmed by DLVO calculation. These results have important implications for prediction of the stability and fate of nanoparticles in natural water.

© 2011 Elsevier B.V. All rights reserved.

1. Introduction

TiO_2 nanoparticles, one of the most popular metal oxide nanoparticles, have been widely used in commercial applications such as photocatalysts, ceramic membranes, paints, sunscreens, and even food [1,2]. The massive applications of TiO_2 nanoparticles in different fields will inherently result in their release into the environment and thereby lead to the exposure of organisms [3]. Based on the potential environmental risk [4], it is important to quantify the environmental fate and transport behavior of TiO_2 nanoparticles. Recently, much attention has been given to the effects of aqueous chemistry on the aggregation and sedimentation behavior of TiO_2 nanoparticles, including ionic strength, cation valence, pH and natural organic matters (NOMs) [1,5–7]. However, there is still a need to understand the mobility and stability of TiO_2 nanoparticles in complex aqueous matrices, because heavy metals, NOMs and other pollutants often present simultaneously in the real environment.

NOMs, ubiquitous in natural water, are shown to have significant effects on the stability of particles in aquatic environment, such as inorganic colloids [8,9], carbon nanotubes [10], and different kinds of nanoparticles [11–13]. The enhanced stabilizing propensity in the presence of NOMs could be attributed to its adsorption on the particle surface, which will reduce the agglomeration of particles due to increased electrostatic repulsion and steric hindrance [2,11–13]. Among the fractions of NOMs, fulvic acids (FA), comprise the major organic constituents (up to 30–50%) in aquatic environments [14]. FA has high carbon content (50–60%) of both aliphatic and aromatic character and various oxygen-containing functional groups (such as carboxylic, phenolic, alcoholic and quinoid groups) [15]. Therefore, the presence of FA may have great influence on the fate and transport of nanoparticles. However, there are few published studies investigating the interaction between FA and TiO_2 nanoparticles [11].

A number of studies have shown the destabilization effect of electrolytes on aggregation of nanoparticles in aqueous environments [1,7,16]. However, most of the previous work focused on the effect of monovalent cations (i.e. Na^+) and divalent cations (i.e. Ca^{2+}, Mg^{2+}) as background ions in the absence and presence of NOMs [2,17–19], and little research has investigated the interaction between nanoparticles and other inorganic ions. Ferric ions (Fe(III)), as one of the most benign species, is a prevalent constituent in natural water and wastewater. Its concentration is at the μg/L level in drinking water [20] and natural river water [21], mg/L level in wastewater [22]. The speciation, solubility and transport of ferric ions depend on a number of factors including the

* Corresponding author. Tel.: +86 10 62767014; fax: +86 10 62767014.
  E-mail address: wlsun@pku.edu.cn (W.L. Sun).

general composition of the water as well as the presence of metal complexing ligands [23–25]. Furthermore, ferric ions are always involved in TiO$_2$ photochemical degradation of the organic pollutants due to the light-absorbing effect of Fe(III)-hydroxy complexes [26,27] and generation of HO$^\bullet$ radicals under UV light [28,29]. Noteworthily, some studies reported the adsorption of ferric ions [30] and Fe(III)-hydroxy complexes [31] on the TiO$_2$ surface in the photocatalytic system before irradiation. However, surface properties of TiO$_2$ nanoparticles in the presence of ferric ions have rarely been studied yet, and experimental studies to systematically delineate the influence of ferric ions on aggregation and sedimentation of TiO$_2$ nanoparticles in the presence and absence of NOMs are lacking.

The objective of this paper is to examine the influence of FA or/and Fe(III) on the aggregation and sedimentation behavior of TiO$_2$ nanoparticles. Particular attention was paid on the combined effect of Fe(III) and FA on the stability of TiO$_2$ suspensions in terms of zeta potential, size and morphology of the resulting aggregates, together with the sedimentation rate at different pH values. DLVO theory was employed to evaluate the observed behaviors. The results will therefore be greatly useful to provide the fundamental information for understanding the stability of nanoparticles in natural water.

2. Experimental

2.1. Materials

Titanium dioxide (P25, Degussa, Germany) was used as received. This TiO$_2$ powder consists of non-porous spheres with an average diameter of 30 nm and specific area of 35–45 m^2/g [32]. Standard Suwannee River fulvic acid (SRFA) (1S101F) was purchased from the International Humic Substances Society, with C element composition 52.44%. The SRFA stock solution was prepared by dissolving 10.0 mg SRFA in 100 mL Milli-Q water and stirring the solution for 24 h. A 20 mM stock solution of FeCl$_3$·6H$_2$O was prepared in Milli-Q water. Both stock solutions were stored in the dark at 4 °C until use. Milli-Q water (18 MΩ) and analytical reagent grade chemicals were used throughout the experiments.

2.2. Experimental design

Aqueous suspensions of TiO$_2$ nanoparticles (50 mg/L) were prepared in a NaCl suspension adjusted to an ionic strength of 5 mM, followed by 30 min of sonication. The effects of SRFA or/and Fe(III) on aggregation and sedimentation behavior of TiO$_2$ were performed in mono-system with SRFA (0–5 mg/L as TOC) or Fe(III) (0–0.20 mM), and binary system with SRFA (at 0.5 or 2.5 mg/L) and Fe(III) (0–0.20 mM), respectively. The solutions containing both SRFA and Fe(III) were magnetically stirred for 1 h before adding to the TiO$_2$ suspension. The mixed solutions of SRFA or/and Fe(III) and TiO$_2$ nanoparticles were stirred at 200 rpm at room temperature for 24 h. The pH values were adjusted to 4.00 ± 0.05, 6.00 ± 0.05 and 8.00 ± 0.05, respectively, with 0.1 M HCl or NaOH. The corresponding zeta potential, particle size and sedimentation of TiO$_2$ nanoparticles were measured after equilibration. TiO$_2$ samples were separated from the solution by centrifugation at 15,000 rpm for 10 min, followed by water washing and ambient temperature drying to yield powder for further characterization.

2.3. Instrumentation and analysis

2.3.1. Zeta potential and particle size measurements

Dynamic light scattering (DLS) measurements were made to determine the zeta potential and hydrodynamic particle size of suspended TiO$_2$ nanoparticles using a Zetasizer Nano ZS90 (Malvern Instruments Ltd., Malvern, UK). The zeta potential was calculated from the electrophoretic mobility using the Smoluchowski model [33]. The particle hydrodynamic diameter was calculated from the diffusion coefficient using the Stokes–Einstein equation [34]. The measurements were performed at 25 °C with an equilibration time of 2 min in an automatic mode. Each sample was measured at least 5 times for particle size and 10 times for zeta potential.

2.3.2. UV–visible absorbance

The sedimentation process of TiO$_2$ nanoparticles was determined by monitoring the optical absorbency at 345 nm using UV–vis spectroscopy (UV-1800, Shimadzu, Japan). Optical absorbency was recorded every 1 min for 600 min.

2.3.3. Transmission electron microscopy (TEM)

The morphology of the particles was studied using a FEI Tecnai G2 T20 analytical transmission electron microscopy (TEM) equipped with energy dispersive X-ray spectrometer (EDX) operating at 200 kV. One drop of the TiO$_2$ sample dispersion was placed on a carbon support copper film substrate (Emerging Red Ltd., Beijing, China), followed by ambient drying for approximately 5 min before TEM analysis.

2.3.4. Fourier-transform infrared (FTIR) spectra

The FTIR spectra were recorded with a FTIR spectrometer (Tensor 27, Bruker, Germany). About 1 mg dry powdered sample was mixed gently with 100 mg KBr as a background, followed by being pressed into translucent sheet. The FTIR spectra were recorded from 400 to 4000 cm^{-1} at 1.0 cm^{-1} interval in transmission mode.

2.3.5. X-ray photoelectron spectroscopy (XPS) analysis

The XPS data were taken on an AXIS-Ultra instrument from Kratos Analytical (UK) using monochromatic Al Kα radiation (225 W, 15 mA, 15 kV) and low-energy electron flooding for charge compensation. To compensate for surface charges effects, binding energies were calibrated using C 1s hydrocarbon peak at 284.80 eV. The data were converted into VAMAS file format and imported into CasaXPS software package for manipulation and curve-fitting.

2.3.6. Determination of sedimentation rates

The sedimentation rates of the TiO$_2$ particles could be measured by the change of optical absorbance with time, which can be related to the normalized nanoparticle concentration C/C_0, where C is the concentration in time t, and C_0 is the initial concentration (i.e. the initial absorbance at time 0). The sedimentation rate is then d(C/C_0)/dt [6]. For relatively fast sedimentation conditions, the initial sedimentation rate is estimated from the decrease in the normalized particle concentration within the first 60 min, while for slower sedimentation conditions (C/C_0 decrease less than 80% in 600 min), all data within 600 min is included.

2.3.7. DLVO particle–particle interaction energy

The DLVO (Derjaguin–Landau–Verwey–Overbeek) theory was employed in this study to calculate the total interaction force between TiO$_2$ nanoparticles under various aqueous conditions. The DLVO total interaction energy (V) is a summation of van der Waals (vdW) attraction (V_{vdW}) and electric double layer (EDL) repulsion (V_{EDL}) [35]:

$$V = V_{vdW} + V_{EDL} \tag{1}$$

$$V_{vdw} = -\frac{A}{6}\left[\frac{2a^2}{s(4a+s)} + \frac{2a^2}{(2a+s)^2} + \ln\frac{s(4a+s)}{(2a+s)^2}\right] \tag{2}$$

$$V_{EDL} = 2\pi\varepsilon a\zeta^2 \, \ln(1 + e^{-\kappa s}) \tag{3}$$

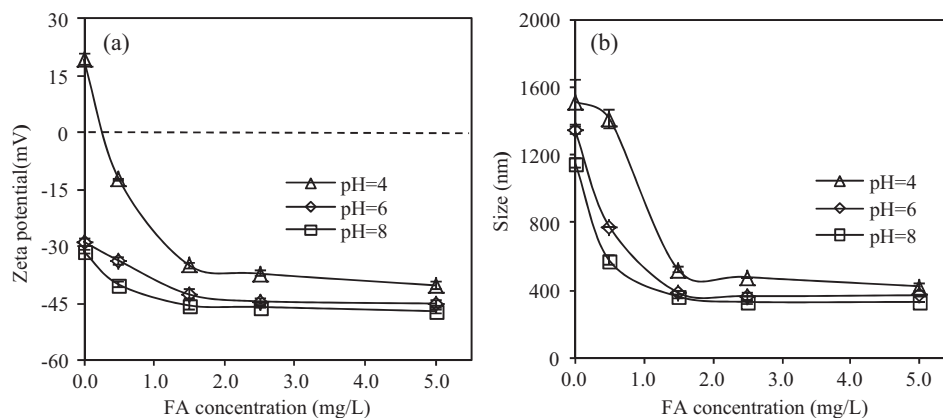**Fig. 1.** Zeta potential (a) and particle size (b) of TiO$_2$ nanoparticles in mono-system of SRFA at pH 4, 6 and 8. Error bars are standard deviations. I = 5 mM NaCl.

where A (6.5×10^{-20} J) is the Hamaker constant of TiO$_2$ in water [36,37]; a (m) is the radius of particles; s (m) is the distance between surfaces of two interacting particles; $\varepsilon = \varepsilon_r \varepsilon_0$ is the dielectric constant, where ε_r (78.54) is the dielectric constant of water and ε_0 (8.85×10^{-12} C^2 J^{-1} m^{-1}) is the permittivity of vacuum; ζ (V), the zeta potential of the charged particles, is assumed to equal the surface potential [35]; κ (m^{-1}) is the reciprocal of the thickness of the double layer and $\kappa = 2.32 \times 10^9$ ($\Sigma C_i Z_i^2$)$^{1/2}$ where C_i is the concentration of ion i and Z_i is its valency value.

3. Results and discussion

3.1. Aggregation/sedimentation of TiO$_2$ nanoparticles in mono-system of SRFA

3.1.1. Zeta potential and particle size measurements

A sharp decrease was observed when the SRFA concentration increased from 0 to 1.5 mg/L, with zeta potential from 19.2 ± 1.4 mV to −35.0 ± 0.6 mV at pH 4, from −28.8 ± 1.0 mV to −42.7 ± 1.3 mV at pH 6, and from −31.4 ± 0.4 mV to −45.6 ± 1.2 mV at pH 8, respectively. Further increase in SRFA concentration resulted in no significant change in zeta potential. Similar observation has also been reported by Zhang et al. [5], in which with the addition of 2 mg/L NOMs, negative zeta potentials of TiO$_2$ nanoparticles were greater than −30 mV while the zeta potentials showed little additional change with NOMs concentration above 2 mg/L.

It has been assumed that, under pure electrostatic interaction, a suspension that exhibits a zeta potential within ±15 mV is considered unstable and tends to aggregate, from ±15 mV to ±30 mV it would be predominantly stable, and above ±40 mV it would be well stabilized [7]. As a result, the addition of SRFA resulted in a sharp decrease in the zeta potential and a great improvement in the stability of the TiO$_2$ solution. This indicates that the properties of the TiO$_2$ nanoparticles were significantly modified by SRFA [11].

Rapid agglomeration of TiO$_2$ nanoparticles was found in aqueous suspension. The initial particle sizes of TiO$_2$ were 1514 ± 131 nm, 1342 ± 23 nm and 1152 ± 32 nm at pH 4, 6 and 8, respectively (Fig. 1b). Micron-sized aggregates of TiO$_2$ were also observed in other researches [1,6]. However, TiO$_2$ nanoparticle sizes decreased with rising SRFA concentrations at pH of 4, 6, and 8 (Fig. 1b). This is in accordance with the increase in the absolute value of surface charge and the subsequent increase in the electrostatic repulsion among TiO$_2$ nanoparticles. The smallest nanoparticle sizes were detected at 5 mg/L SRFA, which were 424 ± 22 nm, 372 ± 1 nm and 332 ± 1 nm at pH 4, 6 and 8, respectively. Zhang

et al. [5] and von der Kammer et al. [7] also demonstrated the stabilization of TiO$_2$ nanoparticles aggregates of a few 100 nm by NOMs.

3.1.2. Sedimentation characterization

TiO$_2$ nanoparticles settled fast out of the suspension in the absence of SRFA, with sedimentation rates 4.4×10^{-3} min^{-1} at pH 4, 3.2×10^{-3} min^{-1} at pH 6, and 2.7×10^{-3} min^{-1} at pH 8, respectively. When SRFA was present in suspensions, sedimentation rates decreased rapidly under all pH values studied (Fig. 2). This is consistent with the zeta potentials and aggregate hydrodynamic diameters measured by DLS analysis (Fig. 1). The results also indicate very stable dispersions of TiO$_2$ when the SRFA concentration was above 1.5 mg/L, with C/C_0 decrease less than 20% in 600 min (Fig. 2a–c). A similar low rate of sedimentation was observed for TiO$_2$ when the aggregate size remained stable at slightly above 300 min a high TOC aqueous matrix [6].

The increased stabilization of TiO$_2$ nanoparticles in the presence of humic substances has been attributed to the electrostatic repulsion [2,12] and steric hindrance [11,17], which is caused by NOMs adsorption on nanoparticles. FA carry many functional groups, including major species such as carboxylic (−COOH) and phenolic (−OH). The interaction of these highly reactive polar groups with the surface active sites of nanoparticles resulted in the adsorption of humic substances [12,13,38], which could modify the surface charges of the nanoparticles.

The TEM images showed that the single TiO$_2$ particles with clear bounds aggregated to a larger particle in the absence of SRFA (Fig. 3a). However, single TiO$_2$ particles were coated and the clear bounds completely disappeared in the presence of SRFA (Fig. 3b), indicating SRFA adsorption on particle surface. Energy dispersive X-ray (EDX) analysis showed peaks of O and Ti elements. Although O peaks may be attributed to TiO$_2$ particles as well as the supporting copper grid, the remarkable increase of O peak in the SRFA–TiO$_2$ sample verified SRFA adsorption onto TiO$_2$ surface (Fig. 3b).

The chemical states and the binding energies of each element in the samples were determined by XPS. The main peaks at binding energy of 284, 458, and 529 eV corresponded to the C 1s, Ti 2s, and O 1s (Fig. 4a), respectively. The high resolution XPS spectra of the TiO$_2$ and SRFA–TiO$_2$ samples at Ti 2p (b), C 1s (c) and O 1s (d) core levels are also shown in Fig. 4. Two prominent peaks were observed at 458.53 eV and 464.23 eV binding energy for the TiO$_2$ sample (Fig. 4b), which are respectively due to Ti 2p$_{3/2}$ and Ti 2p$_{1/2}$ of Ti^{4+} [39,40]. Similar peaks are observed at 458.64 eV and 464.44 eV binding energies for the SRFA–TiO$_2$ sample (Fig. 4b). The
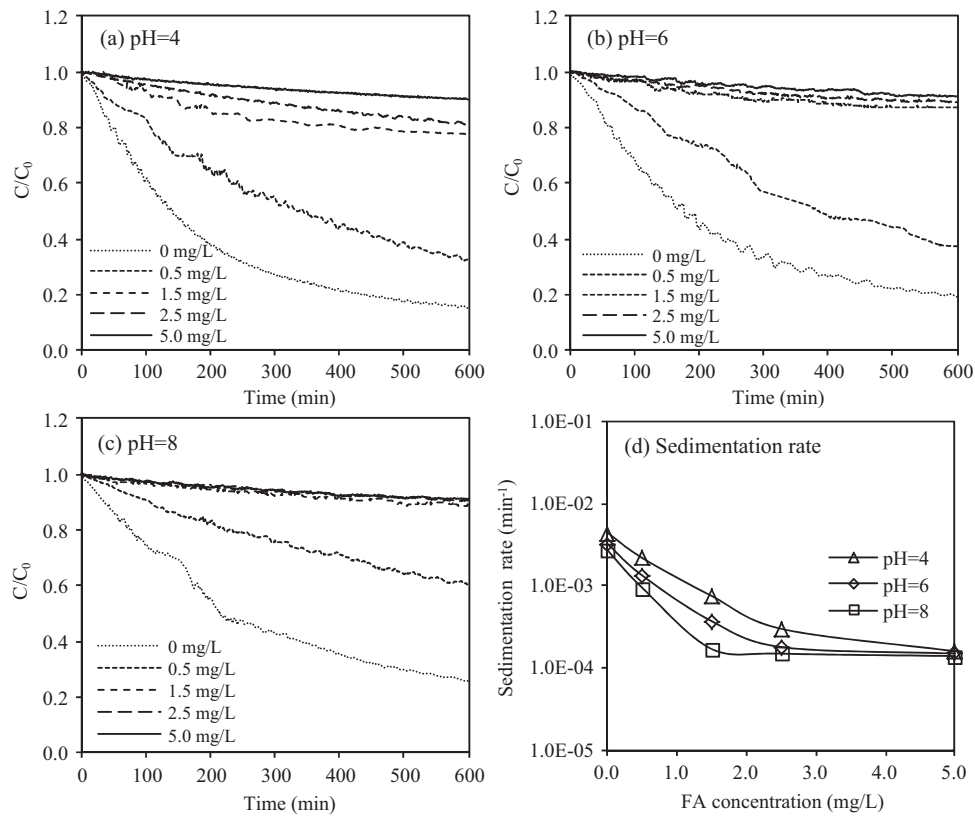
Fig. 2. Sedimentation of TiO$_2$ nanoparticles in mono-system of SRFA at pH 4, 6 and 8. I = 5 mM NaCl.

shift of the Ti 2p$_{3/2}$ indicates the change of TiO$_2$ surface structure with the adsorption of SRFA. The high resolution XPS C 1s spectrum is resolved into three individual component peaks: C–C (charge referenced to 284.80 eV), CO (286.32 eV) and COO (288.73 eV) [15]. Three high resolution O 1s peaks positioned at 529.70, 531.12 and

532.82 eV (Fig. 4d) were assigned to Ti–O–Ti bond [40,41], bridging OH [15] and COO groups [15,41], respectively. The relative intensity of the last two carbon groups and the last oxygen group increased in the SRFA–TiO$_2$ sample (Fig. 4c), indicating that the functional groups of SRFA are introduced in TiO$_2$.
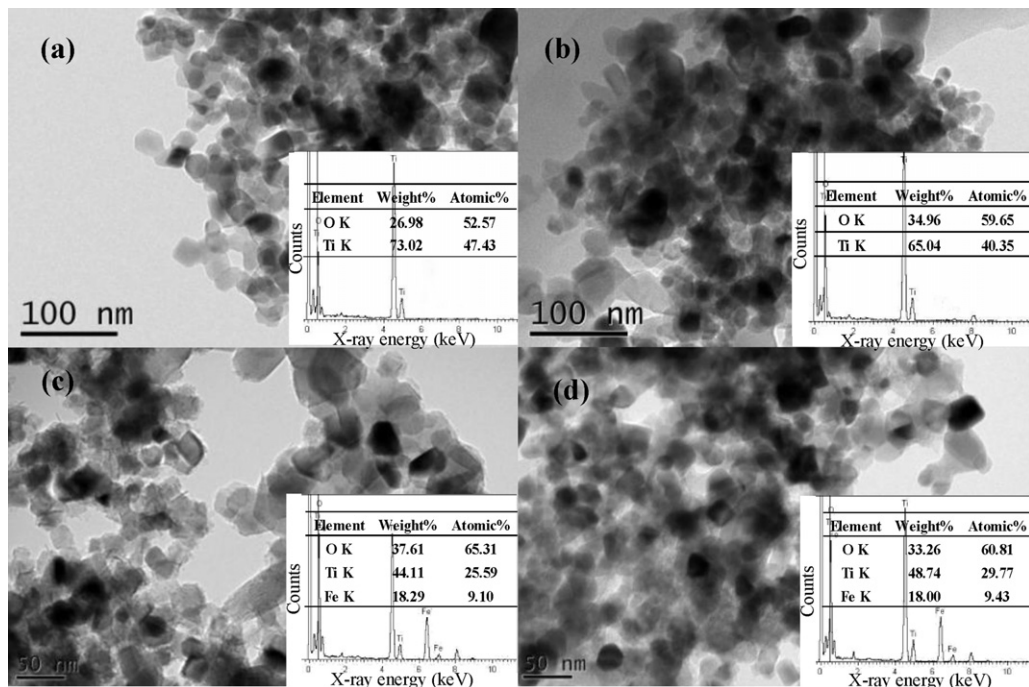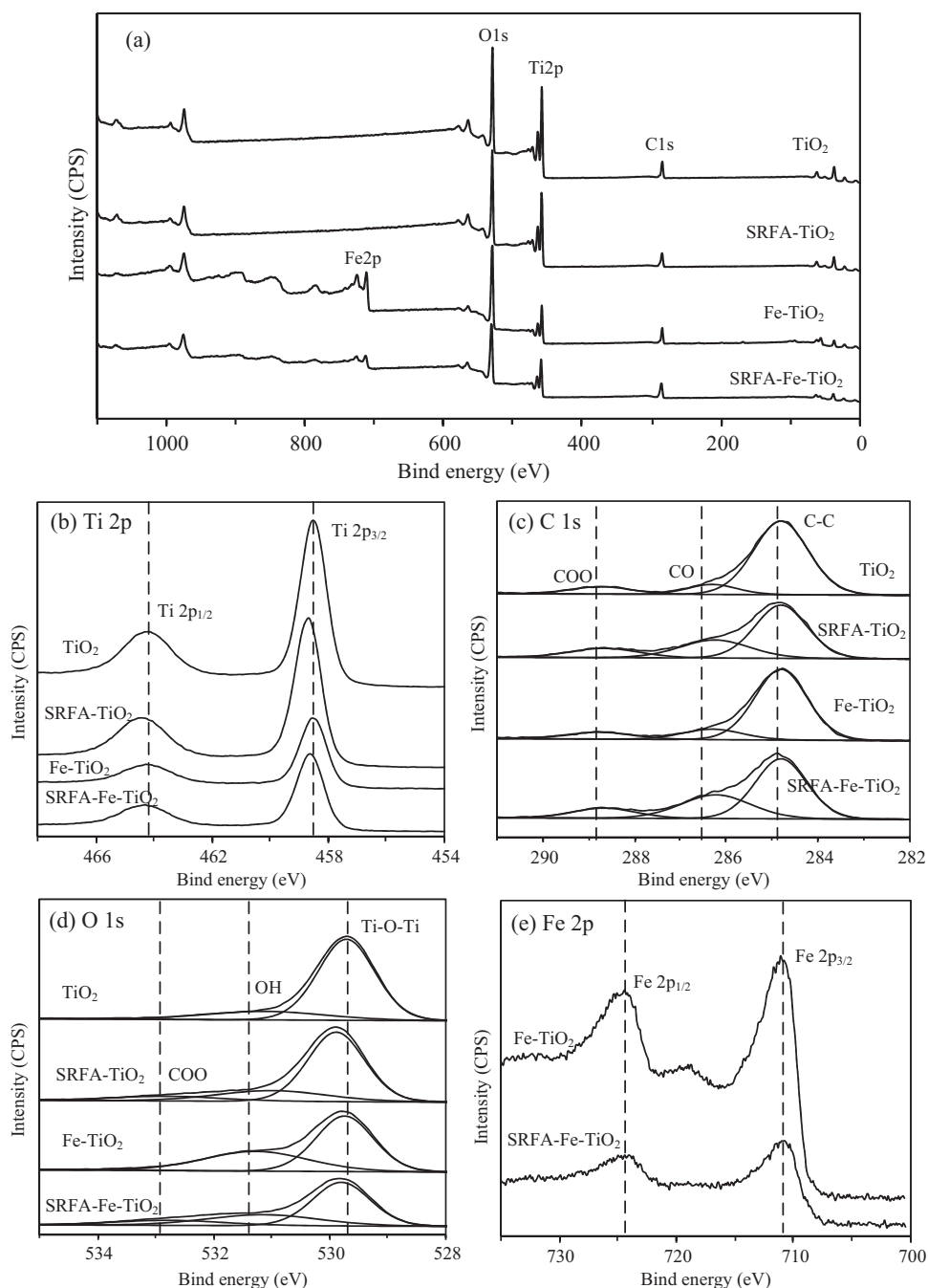

Fig. 3. Representative TEM images and energy dispersive X-ray (EDX) analysis of TiO$_2$ (a), SRFA–TiO$_2$ (b), Fe(III)–TiO$_2$ (c) and SRFA–Fe(III)–TiO$_2$ (d). SRFA = 2.5 mg/L, Fe(III) = 0.20 mM, I = 5 mM NaCl, pH = 6.00 ± 0.05.

Fig. 4. Representative XPS spectra of survey (a), Ti 2p (b), C 1s (c), O 1s (d) and Fe 2p (e) of TiO_2, SRFA–TiO_2, Fe–TiO_2 and SRFA–Fe–TiO_2. SRFA = 2.5 mg/L, Fe(III) = 0.20 mM, I = 5 mM NaCl, pH = 6.00 ± 0.05.

3.2. Aggregation/sedimentation of TiO_2 nanoparticles in mono-system of Fe(III)

3.2.1. Zeta potential and particle size measurements

The increasing Fe(III) concentration resulted in an increase in the zeta potential of TiO_2 nanoparticles under given pH values (Fig. 5a), which was ascribed to the adsorption of Fe(III) on TiO_2 surface [42]. Specifically, at pH 4, the positive charges on TiO_2 nanoparticles increased with increasing Fe(III) concentrations. Meanwhile, negatively charged TiO_2 under pH 6 and 8 became less negative and even positive with increasing Fe(III) concentrations. In addition, most values of the zeta potential were within ±15 mV at pH

6 and 8, indicating that the suspension was unstable and particles would settle out of solution [7].

The particle sizes of TiO_2 decreased at pH 4 while increased at pH 6 and 8 with increasing Fe(III) concentrations (Fig. 5b). At pH 4, aggregation was prevented due to the strong electrostatic repulsion among the nanoparticles. TiO_2 particle sizes were in the range of 287 ± 5 nm to 357 ± 14 nm with the Fe(III) concentration higher than 0.02 mM (Fig. 5b). In contrast, severe aggregation to micro-scale particles occurred at pH 6 and 8 (Fig. 5b). It could be attributed to the decrease in particle–particle repulsion as the zeta potential was within ±15 mV (Fig. 5a) [7]. However, it should be noted that TiO_2 nanoparticles exhibited a high degree
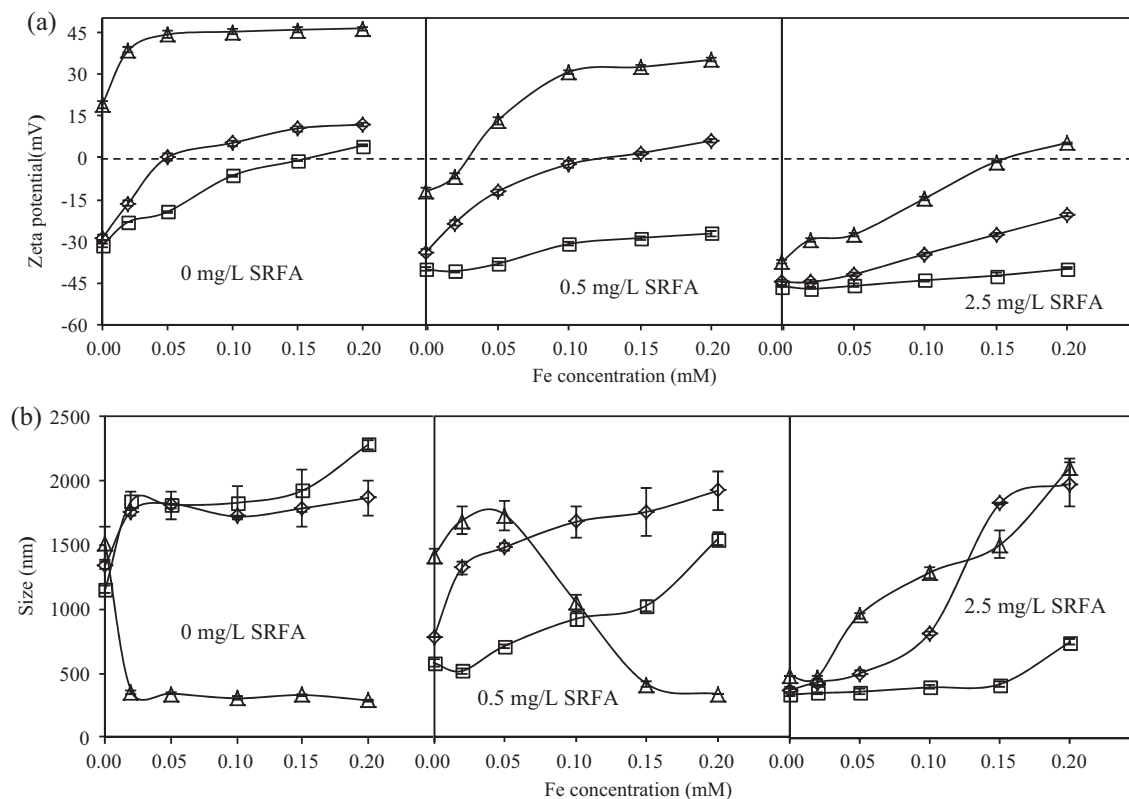
Fig. 5. Zeta potential (a) and particle size (b) of TiO$_2$ nanoparticles in mono-system of Fe(III) and binary system of SRFA and Fe(III) at pH 4 ($\triangle$), 6 ($\diamond$) and 8 ($\square$). Error bars are standard deviations. I = 5 mM NaCl.

of aggregation at pH 6 and 8 even though the measured positive charges increased (Fig. 5a). Enhancement in the aggregation process could be attributed to the formation of Fe(III)-hydroxy colloids. It is well known that hydroxide colloids (Fe(OH)$_3$) are the predominant species of Fe(III) in the solution at pH > 5 [27]. The bridging effect of Fe(III)-hydroxy colloids dominated over electrostatic repulsion to generate larger aggregates at higher pH values.

As shown in the TEM images of TiO$_2$ (Fig. 3c), some needle-like and fusiform materials appeared in the Fe–TiO$_2$ sample at pH 6. The EDX spectra of the aggregates showed peaks of O, Ti and Fe. The appearance of Fe peak and the remarkable increase of O peak may attribute to the presence of Fe(III)-hydroxy complexes in the aggregates. The XPS spectrum of the Fe–TiO$_2$ sample is shown in Fig. 4a. Besides the peaks of Ti 2p (Fig. 4b) and C 1s (Fig. 4c), the characteristic peak of Fe 2p appeared at 711 eV in the Fe–TiO$_2$ sample, corresponding to Fe^{3+} state, verifying its adsorption onto TiO$_2$ surface. The high resolution peaks at 711.67 and 725.07 eV in Fig. 4e were corresponding to binding energy of Fe 2p$_{3/2}$ and Fe 2p$_{1/2}$ of Fe^{3+}, consistent with the values reported in previous literatures [43,44]. Meanwhile, the peak at 531.12 eV (assigned to the bridging OH) [15] obviously increased in the Fe–TiO$_2$ sample, implying the formation of Fe(III)-hydroxy complexes.

3.2.2. Sedimentation characterization

Similar to SRFA (Fig. 2d), the addition of Fe(III) stabilizing the aggregation of TiO$_2$ nanoparticles, the sedimentation rates decreased from 2.3×10^{-4} min^{-1} to 1.2×10^{-4} min^{-1} with increasing Fe(III) concentrations from 0 to 0.20 mM at pH 4 (Fig. 6g). In contrast, the sedimentation rates increased with increasing Fe(III) concentrations at pH 6 and 8 (Fig. 5b). The maximum sedimentation rates, 7.0×10^{-3} min^{-1} at pH 6 and 1.1×10^{-2} min^{-1} at pH 8, were observed at 0.20 mM Fe(III).

3.3. Aggregation/sedimentation of TiO$_2$ nanoparticles in binary system of SRFA and Fe(III)
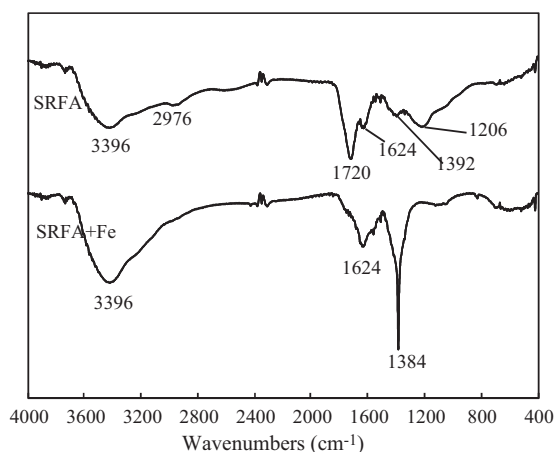
3.3.1. Zeta potential and particle size measurements

Similar with those in mono-system of Fe(III), the zeta potentials of TiO$_2$ increased with increasing Fe(III) concentrations in the presence of SRFA (Fig. 5a). However, the increasing amount of zeta potentials differed at three given pH values. At pH 4, the increasing amounts of zeta potentials were 47.4 mV (-12.3 ± 0.2 mV to 35.1 ± 0.7 mV) and 42.6 mV (-37.2 ± 0.8 mV to 5.4 ± 0.3 mV) at SRFA concentrations of 0.5 and 2.5 mg/L, respectively, as Fe(III) concentration increased from 0 to 0.20 mM. A smaller increasing amount of zeta potentials, 27.2 mV (19.2 $\pm$ 1.4 mV to 46.4 $\pm$ 0.7 mV), was found in the absence of SRFA. Zeta potentials increased 40.7 mV, 39.9 mV, and 23.8 mV by 0.20 mM Fe(III) at SRFA concentrations of 0 mg/L, 0.5 mg/L and 2.5 mg/L, respectively, and pH 6. The corresponding increasing amounts of zeta potential at pH 8 were 35.8 mV, 12.9 mV and 6.2 mV, respectively. The results showed that the increasing amounts of zeta potentials of TiO$_2$ nanoparticles decreased with increasing SRFA concentrations except for the condition of pH 4 in the absence of SRFA, indicating the effect of Fe(III) on zeta potentials of TiO$_2$ nanoparticles decreased due to addition of SRFA. This could be attributed to the complexation of Fe(III) with SRFA, which was verified by FTIR analysis (Fig. 7). The band at 1720 cm^{-1} in SRFA FTIR spectra, which was generally attributed to C=O stretching of carboxylic groups [45], disappeared in the spectra of SRFA–Fe(III) complex while a strong peak at 1384 cm^{-1} appeared. This new peak was consistent with a COO–Fe(III) stretching reported by previous studies [25,46,47]. Similarly, Thio et al. [2] reported that increasing Ca^{2+} concentrations had much less effect on surface charge of TiO$_2$ nanoparticles in the presence of humic acid (HA) due to Ca^{2+} binding to the carboxylic functional groups of HA [18,48].
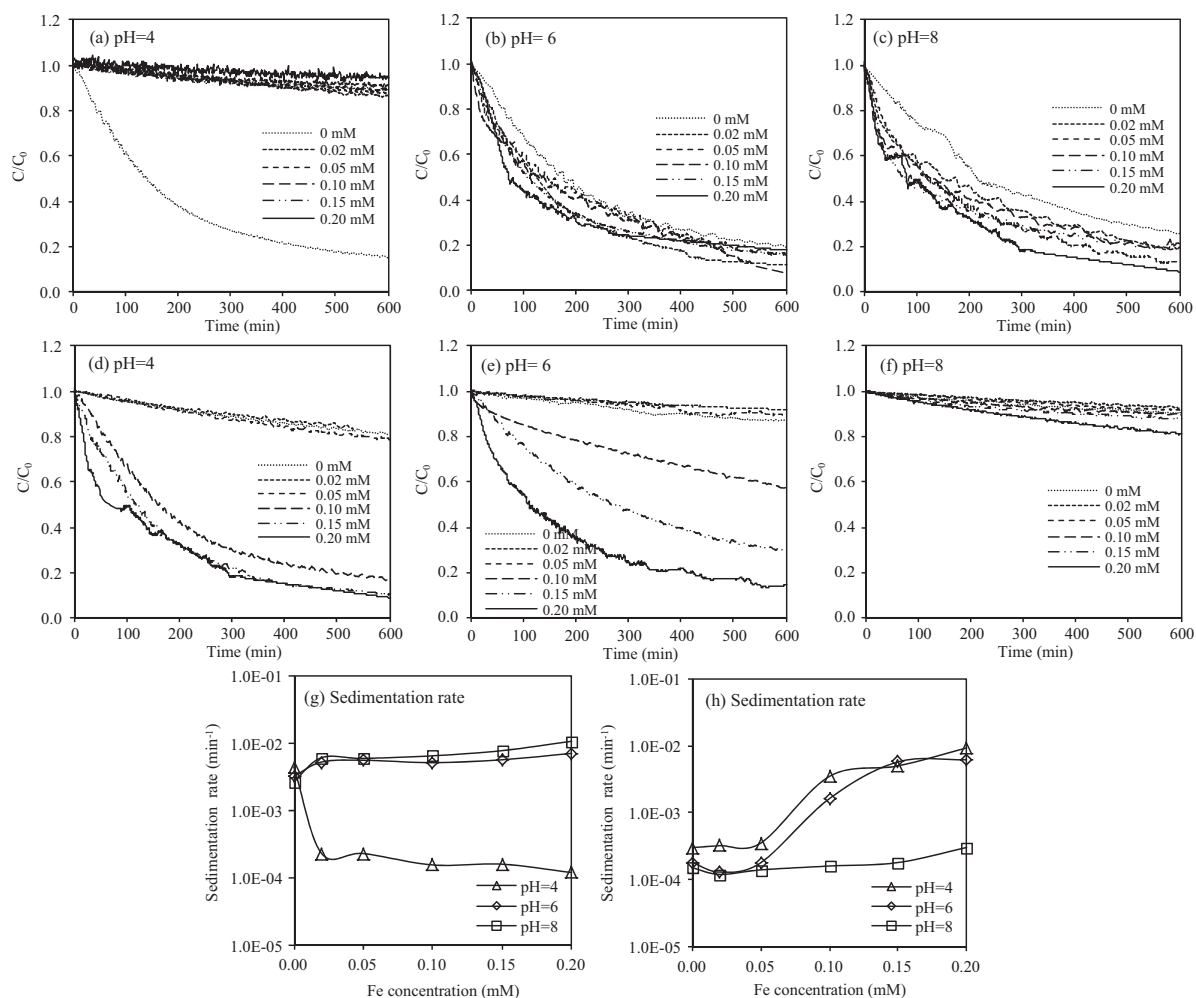
Fig. 6. Sedimentation of TiO$_2$ nanoparticles in mono-system of Fe(III) (a–c and g) and binary system of SRFA (2.5 mg/L) and Fe(III) (d–f and h) at pH 4, 6 and 8. I = 5 mM NaCl.

At pH 4, TiO$_2$ particle sizes increased at low Fe(III) concentrations and then decreased rapidly with Fe(III) concentration higher than 0.05 mM in the presence of 0.5 mg/L SRFA, while a continuously rising in the particle sizes was observed in the presence of 2.5 mg/L SRFA. Compared with the decreasing TiO$_2$ particle sizes in mono-system of Fe(III), the addition of SRFA weaken or contravened the stabilizing effect of Fe(III) at pH 4. Meanwhile, reduced

Fig. 7. FTIR spectra of FA–Fe (III) complex. SRFA = 2.5 mg/L, Fe = 0.10 mM, I = 5 mM NaCl, pH = 6.00 ± 0.05.

aggregation effect was found in binary system of SRFA and Fe(III) at pH 6 and 8 compared with that in mono-system of Fe(III) (Fig. 5b). These results suggested that SRFA complexing with Fe(III) could reduce the effect of Fe(III) on TiO$_2$ nanoparticles at all pH values studied. Enhanced aggregation in the presence of Ca^{2+} and HA at pH 4 was also observed by Liu et al. [19] attributed to the bridging effect of HA aggregates. Moreover, the stabilization effect of HA in the Ca^{2+} solution at pH 5.6 and 8 was reported in previous studies [2,18], in which the critical coagulation concentration for Ca^{2+} increased in the presence of HA.

### 3.3.2. Sedimentation characterization

In general, the sedimentation rates increased with the increasing Fe(III) concentration in the presence of SRFA (Fig. 5). The maximum sedimentation rates were 9.3×10^{-3} min^{-1} at pH 4, 6.2×10^{-3} min^{-1} at pH 6, 3.0×10^{-4} min^{-1} at pH 8, respectively, with 0.20 mM Fe(III) (Fig. 6h). Compared with those in mono-system of Fe(III), the above mentioned sedimentation rates increased by 76.5 times at pH 4 while decreased by 11.4% and 97% at pH 6 and 8, respectively (Fig. 6g and h). This may indicate that no or less Fe(III)-hydroxy colloids formed at pH 6 and 8 in the presence of SRFA.

TEM image of TiO$_2$ nanoparticles in binary system of SRFA and Fe(III) in 5 mM NaCl solution at pH 6 is presented in Fig. 3d. The boundaries in the single TiO$_2$ particles became indistinct with SRFA and Fe(III) addition, which could be attributed to the SRFA–Fe(III) complex adsorbed on TiO$_2$ surface. The adsorption of SRFA–Fe(III)
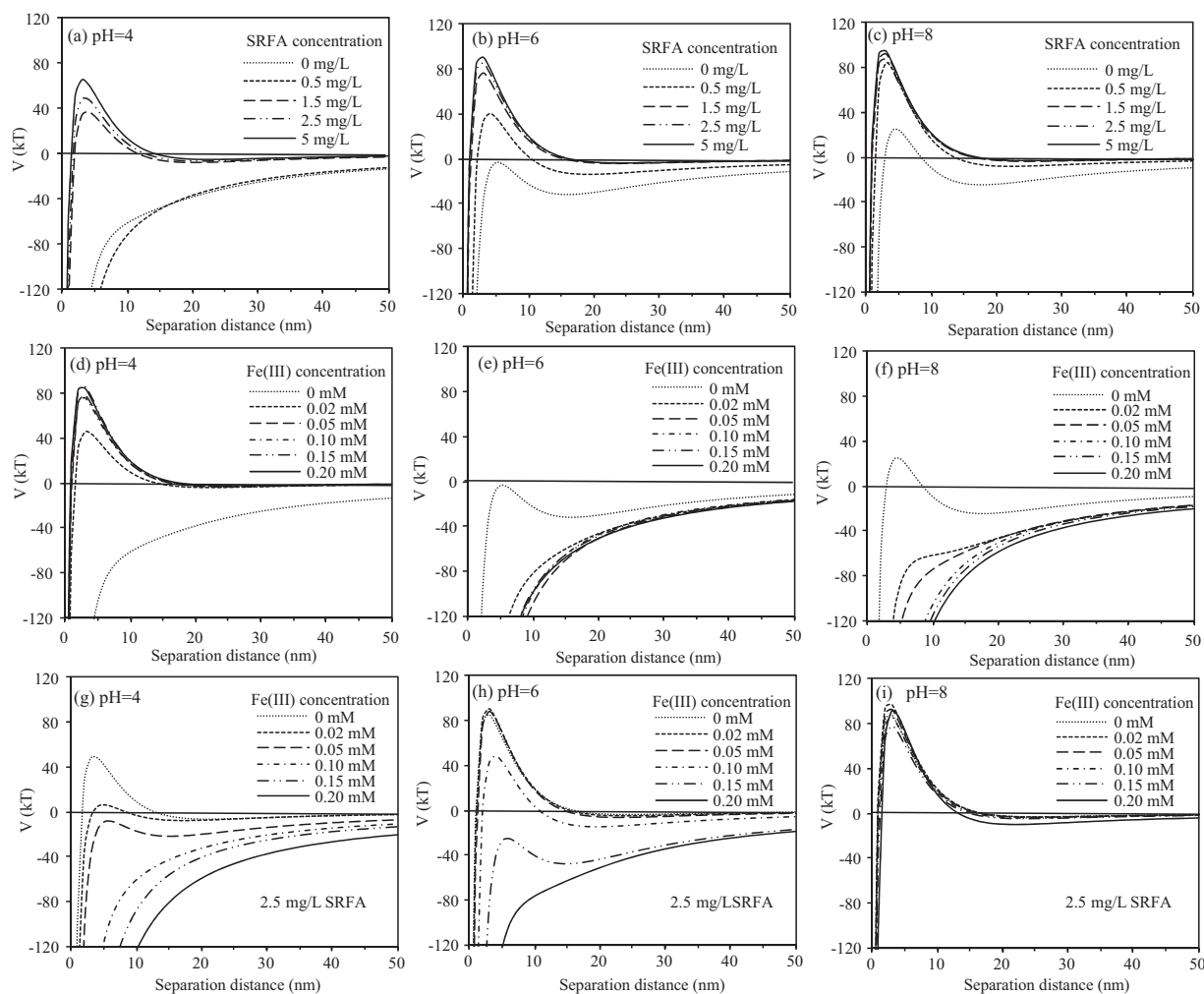
Fig. 8. DLVO interaction energy between TiO$_2$ nanoparticles versus separation distance in mono-system of SRFA (a–c), Fe(III) (d–f), and binary system of SRFA (2.5 mg/L) and Fe(III) (g–i). I = 5 mM NaCl.

complex was verified by EDX analysis. Three peaks of O, Ti and Fe were present in the SRFA–Fe–TiO$_2$ sample and the intensity of O peak increased remarkably compared to the TiO$_2$ sample.

The XPS spectrum of TiO$_2$ nanoparticles in binary system of SRFA and Fe(III) were shown in Fig. 4a. Four main peaks ascribed to C 1s, Ti 2s, O 1s and Fe 2p were present in the SRFA–Fe–TiO$_2$ sample. The relative intensity of the CO (286.32 eV) and COO (288.73 eV and 532.82 eV) [15] increased in the SRFA–Fe–TiO$_2$ sample (Fig. 4c), which indicates that the functional groups of SRFA were introduced in TiO$_2$. The presence of Fe (Fig. 4e) confirmed the adsorption of Fe(III) species on TiO$_2$ surface.

3.4. DLVO evaluation of interactions between TiO$_2$ nanoparticles

The DLVO interactions between TiO$_2$ nanoparticles in mono-system of SRFA (a–c) or Fe(III) (d–f) and binary system of SRFA (2.5 mg/L) and Fe(III) (g–i) were presented in Fig. 8. In the absence of SRFA (Fig. 8a–c), the EDL repulsive energy was relatively small and the net energy between nanoparticles was attractive (except a low net repulsive energy barrier appeared at pH 8), which was favorable for the aggregation of TiO$_2$ nanoparticles. The addition of SRFA imparted negative charges to particle surface and therefore increased the EDL repulsive energy between nanoparticles. The energy barriers increased with increasing SRFA concentrations in most cases (Fig. 8a–c). TiO$_2$ nanoparticles were stabilized, which was in agreement with experimental results (Fig. 1) and

previous studies [5,49]. It should be noted that, DLVO theory predicted increased likelihood for aggregation with 0.5 mg/L SRFA at pH 4 (Fig. 8a). However, the observed decrease in the particle size (Fig. 1b) could be attributed to steric hindrance [11,17] due to the SRFA adsorption. The steric hindrance still existed at higher SRFA concentrations but EDL repulsion dominated instead [9,50].

The interactions between TiO$_2$ nanoparticles changed in different manners with increasing Fe(III) concentrations at different pH (Fig. 8d–f). A dramatic increase in energy barriers were predicted at pH 4, which suggested that the presence of Fe(III) helped to stabilize the TiO$_2$ nanoparticles suspension. In contrast, the energy barriers decreased at pH 6 and 8, indicating increased likelihood for aggregation. The DLVO descriptions were consistent with the particle size measurements in most cases (Fig. 5b). However, when Fe(III) concentrations were higher than 0.10 mM at pH 6, DLVO forces predicted reduced aggregation propensities (Fig. 8e), while particle sizes increased instead (Fig. 5b). The discrepancy suggested that non-DLVO interaction forces played important roles in TiO$_2$ nanoparticles aggregation. This could be attributed to the bridging effect of Fe(III)-hydroxy complex as aforementioned.

In binary system of SRFA and Fe(III), at pH 4, the energy barriers of TiO$_2$ nanoparticles dramatically decreased or even disappeared (Fig. 8g) and TiO$_2$ nanoparticles began to aggregate (Fig. 5b). Similar effects of Ca^{2+} were reported by Zhang et al. [5] for NOM-coated TiO$_2$ nanoparticles. The results were opposite to the increased energy barriers (Fig. 8d) and decreased particle sizes (Fig. 5b)

observed in mono-system of Fe(III). In addition, no energy barriers were found in mono-system of Fe(III) at pH 6 and 8 (Fig. 8e and f) while some relatively high barriers were still present with the addition of SRFA (Fig. 8h and i). This indicates the aggregation was inhibited in the presence of SRFA. Therefore, at all pH values studied, the effect of Fe(III) on the interactions between TiO$_2$ nanoparticles was reduced or even contravened by the addition of SRFA, which was in accordance with zeta potential and particle size measurements (Fig. 5).

3.5. Relationship between sedimentation rates and particle sizes/zeta potentials

Nanoparticles' sedimentation will reduce the stability of nanofluids, thus may limit the application of nanofluids [49]. Jiang et al. [49] reported that the aggregation/sedimentation characteristics of nanoparticles could be predicted when the forces on each nanoparticle were determined. It has also been reported that the extent of transport of TiO$_2$ nanoparticles was highly influenced by both surface potential and the aggregates size [50]. However, little research was related to the sedimentation rates which could be calculated by the sedimentation profile [6]. In present study, Pearson correlation coefficients between sedimentation rates and particle sizes/zeta potentials were calculated using SPSS (PASW Statistics v18.0.0, SPSS Inc., USA). The results showed that sedimentation rates of TiO$_2$ nanoparticles had significant correlations to the particle sizes and absolute zeta potentials ($P < 0.01$), with coefficients 0.964 and −0.883, respectively. Significant correlation between average particle diameter and the fraction CeO$_2$ remaining in suspension ($P < 0.01$) was also found by Quik et al. [51] for studying CeO$_2$ settling in deionized water and algae medium in the presence of different NOMs types and concentrations. These results revealed that particle sizes and zeta potentials were dominant factors influencing the removal of nanoparticles from suspension, irrespectively of the solution chemistry. However, the relatively lower correlation (−0.883) between sedimentation rates and absolute zeta potentials may resulted from non-DLVO interactions as described in the aforementioned results: (1) the bridging effect of Fe(III)-hydroxy colloid in mono-system of Fe(III) at higher pH; (2) and the steric repulsion in the presence of SRFA [11,17].

4. Conclusions

Severe aggregation to micro-scale TiO$_2$ nanoparticles was found in aqueous solution with 5 mM NaCl. However, SRFA adsorption significantly increased the EDL repulsion and produced net energy barriers to aggregation at all pH studied. The particle sizes, correspondingly, dropped to a few 100 nm. In mono-system of Fe(III), particle sizes of TiO$_2$ nanoparticles reduced at pH 4, while increased at higher pH due to the formation of Fe(III)-hydroxy colloid, which resulted in the disagreement with DLVO theory. In binary system of SRFA and Fe(III), aggregation was enhanced at pH 4 while reduced at pH 6 and 8 with addition of SRFA, compared with those in mono-system of Fe(III). The reduced effect of Fe(III) was attributed to the complexation of carboxylic groups in SRFA with Fe(III). All of the observed sedimentation rates had significant correlation to the hydrodynamic diameters of TiO$_2$ nanoparticles with coefficient 0.964 irrespectively of solution composition ($P < 0.01$). Whereas, sedimentation rates showed significant correlation ($P < 0.01$) to zeta potentials with relatively lower coefficient −0.883 due to the non-DLVO interactions resulted from the bridging effect of Fe(III)-hydroxy complex or the steric repulsion in the presence of SRFA.

The results provide a context for understanding the stability and fate of nanoparticles in natural water. NOMs are ubiquitous in surface waters. Nanoparticles will be coated by NOMs when they enter surface waters, resulting in a very stable solution. The particles will not sediment out within a few days. However, a certain amount of multivalent cations, such as ferric ions, in natural water will counteract the stabilizing effect of NOMs on nanoparticles, lead to nanoparticle aggregation, and thus reduce the ecotoxicity of nanoparticles. Therefore, the low level of multivalent cations cannot be ignored when studying the behavior of nanoparticles in natural water, because they give rise to a more sensitive and complicated effect than the predominant cations such as Na$^+$ and Ca^{2+}.

References

[1] R.A. French, A.R. Jacobson, B. Kim, S.L. Isley, R.L. Penn, P.C. Baveye, Influence of ionic strength, pH, and cation valence on aggregation kinetics of titanium dioxide nanoparticles, Environ. Sci. Technol. 43 (2009) 1354–1359.

[2] B.J.R. Thio, D.X. Zhou, A.A. Keller, Influence of natural organic matter on the aggregation and deposition of titanium dioxide nanoparticles, J. Hazard. Mater. 189 (2011) 556–563.

[3] R. Kaegi, A. Ulrich, B. Sinnet, R. Vonbank, A. Wichser, S. Zuleeg, H. Simmler, S. Brunner, H. Vonmont, M. Burkhardt, M. Boller, Synthetic TiO$_2$ nanoparticle emission from exterior facades into the aquatic environment, Environ. Pollut. 156 (2008) 233–239.

[4] A. Menard, D. Drobne, A. Jemec, Ecotoxicity of nanosized TiO$_2$. Review of in vivo data, Environ. Pollut. 159 (2011) 677–684.

[5] Y. Zhang, Y.S. Chen, P. Westerhoff, J. Crittenden, Impact of natural organic matter and divalent cations on the stability of aqueous nanoparticles, Water Res. 43 (2009) 4249–4257.

[6] A.A. Keller, H. Wang, D. Zhou, H.S. Lenihan, G. Cherr, B.J. Cardinale, R. Miller, Z. Ji, Stability and aggregation of metal oxide nanoparticles in natural aqueous matrices, Environ. Sci. Technol. 44 (2010) 1962–1967.

[7] F. von der Kammer, S. Ottofuelling, T. Hofmann, Assessment of the physicochemical behavior of titanium dioxide nanoparticles in aquatic environments using multi-dimensional parameter testing, Environ. Pollut. 158 (2010) 3472–3481.

[8] C.L. Tiller, C.R. O'Melia, Natural organic matter and colloidal stability: models and measurements, Colloids Surf. A: Physicochem. Eng. Aspects 73 (1993) 89–102.

[9] J. Buffle, K.J. Wilkinson, S. Stoll, M. Filella, J.W. Zhang, A generalized description of aquatic colloidal interactions: the three-colloidal component approach, Environ. Sci. Technol. 32 (1998) 2887–2899.

[10] H. Hyung, J.D. Fortner, J.B. Hughes, J.H. Kim, Natural organic matter stabilizes carbon nanotubes in the aqueous phase, Environ. Sci. Technol. 41 (2007) 179–184.

[11] R.F. Domingos, N. Tufenkji, K.J. Wilkinson, Aggregation of titanium dioxide nanoparticles: role of a fulvic acid, Environ. Sci. Technol. 43 (2009) 1282–1286.

[12] K. Yang, D.H. Lin, B.S. Xing, Interactions of humic acid with nanosized inorganic oxides, Langmuir 25 (2009) 3571–3576.

[13] J.D. Hu, Y. Zevi, X.M. Kou, J. Xiao, X.J. Wang, Y. Jin, Effect of dissolved organic matter on the stability of magnetite nanoparticles under different pH and ionic strength conditions, Sci. Total Environ. 408 (2010) 3477–3489.

[14] T. Reemtsma, A. These, A. Springer, M. Linscheid, Differences in the molecular composition of fulvic acid size fractions detected by size-exclusion chromatography – on line Fourier transform ion cyclotron resonance (FTICR-) mass spectrometry, Water Res. 42 (2008) 63–72.

[15] X.L. Tan, X. Fang, J.X. Li, Y. Lu, X.K. Wang, Adsorption of Eu(III) onto TiO$_2$: effect of pH, concentration, ionic strength and soil fulvic acid, J. Hazard. Mater. 168 (2009) 458–465.

[16] A.M. El Badawy, T.P. Luxton, R.G. Silva, K.G. Scheckel, M.T. Suidan, T.M. Tolaymat, Impact of environmental conditions (pH, ionic strength, and electrolyte type) on the surface charge and aggregation of silver nanoparticles suspensions, Environ. Sci. Technol. 44 (2010) 1260–1266.

[17] K.L. Chen, M. Elimelech, Influence of humic acid on the aggregation kinetics of fullerene (C$_{60}$) nanoparticles in monovalent and divalent electrolyte solutions, J. Colloid Interface Sci. 309 (2007) 126–134.

[18] X.Y. Liu, M. Wazne, Y. Han, C. Christodoulatos, K.L. Jasinkiewicz, Effects of natural organic matter on aggregation kinetics of boron nanoparticles in monovalent and divalent electrolytes, J. Colloid Interface Sci. 348 (2010) 101–107.

[19] X.Y. Liu, M. Wazne, T. Chou, R. Xiao, S.Y. Xu, Influence of Ca^{2+} and Suwannee River humic acid on aggregation of silicon nanoparticles in aqueous media, Water Res. 45 (2011) 105–112.

[20] Q.F. Hu, G.Y. Yang, J.H. Yang, J.Y. Yin, Study on determination of iron, cobalt, nickel, copper, zinc and manganese in drinking water by solid-phase extraction

and RP-HPLC with 2-(2-quinolinylazo)-5-diethylaminophenol as precolumn derivatizing reagent, J. Environ. Monit. 4 (2002) 956–959.

[21] J.M. Martin, D.M. Guan, F. Elbaz-Poulichet, A.J. Thomas, V.V. Gordeev, Preliminary assessment of the distributions of some trace elements (As, Cd, Cu, Fe, Ni, Pb and Zn) in a pristine aquatic environment: the Lena River estuary (Russia), Mar. Chem. 43 (1993) 185–199.

[22] J.C. Xu, G. Chen, X.F. Huang, G.M. Li, J. Liu, N. Yang, S.N. Gao, Iron and manganese removal by using manganese ore constructed wetlands in the reclamation of steel wastewater, J. Hazard. Mater. 169 (2009) 309–317.

[23] K. Barbeau, E.L. Rue, K.W. Bruland, A. Butler, Photochemical cycling of iron in the surface ocean mediated by microbial iron(III)-binding ligands, Nature 413 (2001) 409–413.

[24] T. Weber, T. Allard, M.F. Benedetti, Iron speciation in interaction with organic matter: modelling and experimental approach, J. Geochem. Explor. 88 (2006) 166–171.

[25] X.X. Ou, S. Chen, X. Quan, H.M. Zhao, Photochemical activity and characterization of the complex of humic acids with iron(III), J. Geochem. Explor. 102 (2009) 49–55.

[26] S.F. Chen, G.Y. Cao, Study on the photocatalytic reduction of dichromate and photocatalytic oxidation of dichlorvos, Chemosphere 60 (2005) 1308–1315.

[27] S.W. Lam, K. Chiang, T.M. Lim, R. Amal, G.K.-C. Low, The role of ferric ion in the photochemical and photocatalytic oxidation of resorcinol, J. Catal. 234 (2005) 292–299.

[28] V. Brezová, A. Blažková, E. Borošová, M. Čeppan, R. Fiala, The influence of dissolved metal ions on the photocatalytic degradation of phenol in aqueous TiO$_2$ suspensions, J. Mol. Catal. A: Chem. 98 (1995) 109–116.

[29] U. Černigoj, U. Lavrenčič Štangar, J. Jirkovský, Effect of dissolved ozone or ferric ions on photodegradation of thiacloprid in presence of different TiO$_2$ catalysts, J. Hazard. Mater. 177 (2010) 399–406.

[30] T. Ohno, D. Haga, K. Kaijaki, M. Matsumura, Unique effects of iron(III) ions on photocatalytic and photoelectrochemical properties of titanium dioxide, J. Phys. Chem. B 101 (1997) 6415–6419.

[31] M.S. Nahar, K. Hasegava, S. Kagaya, S. Kuroda, Adsorption and aggregation of Fe(III)-hydroxy complexes during the photodegradation of phenol using theiron-added-TiO$_2$ combined system, J. Hazard. Mater. 162 (2009) 351–355.

[32] R.I. Bickley, T. Gonzalez-Carreno, J.S. Lees, L. Palmisano, R.J.D. Tilley, A structural investigation of titanium dioxide photocatalysts, J. Solid State Chem. 92 (1991) 178–190.

[33] K.M. Buettner, C.I. Rinciog, S.E. Mylon, Aggregation kinetics of cerium oxide nanoparticles in monovalent and divalent electrolytes, Colloids Surf. A: Physicochem. Eng. Aspects 366 (2010) 74–79.

[34] I.-L. Hsiao, Y.-J. Huang, Effects of various physicochemical characteristics on the toxicities of ZnO and TiO$_2$ nanoparticles toward human lung epithelial cells, Sci. Total Environ. 409 (2011) 1219–1228.

[35] M. Elimelech, J. Gregory, X. Jia, R. Williams, Particle Deposition and Aggregation: Measurement, Modeling, and Simulation, Butterworth-Heinemann, Boston, USA, 1995.

[36] H.D. Ackler, R.H. French, Y.-M. Chiang, Comparisons of Hamaker constants for ceramic systems with intervening vacuum or water: from force laws and physical properties, J. Colloid Interface Sci. 179 (1996) 460–469.

[37] X.Y. Liu, G.X. Chen, C.M. Su, Effects of material properties on sedimentation and aggregation of titanium dioxide nanoparticles of anatase and rutile in the aqueous phase, J. Colloid Interface Sci. (2011), doi:10.1016/j.jcis.2011.06.085.

[38] S. Sander, L.M. Mosley, K.A. Hunter, Investigation of interparticle forces in natural waters: effects of adsorbed humic acids on iron oxide and alumina surface properties, Environ. Sci. Technol. 38 (2004) 4791–4796.

[39] U.G. Akpan, B.H. Hameed, Enhancement of the photocatalytic activity of TiO$_2$ by doping it with calcium ions, J. Colloid Interface Sci. 357 (2011) 168–178.

[40] H.R. Jafry, M.V. Liga, Q.L. Li, A.R. Barron, Simple route to enhanced photocatalytic activity of P25 titanium dioxide nanoparticles by silica addition, Environ. Sci. Technol. 45 (2011) 1563–1568.

[41] N. Kruse, S. Chenakin, XPS characterization of Au/TiO$_2$ catalysts: binding energy assessment and irradiation effects, Appl. Catal. A: Gen. 391 (2011) 367–376.

[42] K.L. Chen, M. Elimelech, Aggregation and deposition kinetics of fullerene (C$_{60}$) nanoparticles, Langmuir 22 (2006) 10994–11001.

[43] Z. Ambrus, N. Balázs, T. Alapi, G. Wittman, P. Sipos, A. Dombi, K. Mogyorósi, Synthesis, structure and photocatalytic properties of Fe(III)-doped TiO$_2$ prepared from TiCl$_3$, Appl. Catal. B: Environ. 81 (2008) 27–37.

[44] T.K. Ghorai, S.K. Biswas, P. Pramanik, Photooxidation of different organic dyes (RB, MO, TB, and BG) using Fe(III)-doped TiO$_2$ nanophotocatalyst prepared by novel chemical method, Appl. Surf. Sci. 254 (2008) 7498–7504.

[45] D. He, X.H. Guan, J. Ma, M. Yu, Influence of different nominal molecular weight fractions of humic acids on phenol oxidation by permanganate, Environ. Sci. Technol. 43 (2009) 8332–8337.

[46] B. Gu, J. Schmit, Z. Chen, L. Liang, J.F. McCarthy, Adsorption and desorption of natural organic matter on iron oxide: mechanisms and models, Environ. Sci. Technol. 28 (1994) 38–46.

[47] H.B. Fu, X. Quan, Complexes of fulvic acid on the surface of hematite, goethite, and akaganeite: FTIR observation, Chemosphere 63 (2006) 403–410.

[48] S. Yoon, C. Lee, K. Kim, A.G. Fane, Effect of calcium ion on the fouling of nanofilter by humic acid in drinking water production, Water Res. 32 (1998) 2180–2186.

[49] W.T. Jiang, G.L. Ding, H. Peng, H.T. Hu, Modeling of nanoparticles' aggregation and sedimentation in nanofluid, Curr. Appl. Phys. 10 (2010) 934–941.

[50] K.A.D. Guzman, M.P. Finnegan, J.F. Banfield, Influence of surface potential on aggregation and transport of titania nanoparticles, Environ. Sci. Technol. 40 (2006) 7688–7693.

[51] J.T.K. Quik, I. Lynch, K. Van Hoecke, C.J.H. Miermans, K.A.C. De Schamphelaere, C.R. Janssen, K.A. Dawson, M.A. Cohen Stuart, D. Van De Meent, Effect of natural organic matter on cerium dioxide nanoparticles settling in model fresh water, Chemosphere 81 (2010) 711–715.